Article

A New Integrated Tool to Calculate and Map Bilateral Asymmetry on Three-Dimensional Digital Models

Marina Melchionna [1,*,†], Antonio Profico [2,†], Costantino Buzi [3], Silvia Castiglione [1], Alessandro Mondanaro [4], Antonietta Del Bove [5,6], Gabriele Sansalone [7], Paolo Piras [8] and Pasquale Raia [1]

[1] Dipartimento di Scienze della Terra, dell'Ambiente e delle Risorse, Università di Napoli Federico II, 80126 Napoli, Italy; silvia.castiglione@unina.it (S.C.); pasquale.raia@unina.it (P.R.)
[2] PalaeoHub, Department of Archaeology, Hull York Medical School University of York, Heslington YO10 5DD, UK; antonio.profico@york.ac.uk
[3] DFG Centre for Advanced Studies 'Words, Bones, Genes, Tools', Eberhard Karls University of Tübingen, 72070 Tübingen, Germany; costantino.buzi@uni-tuebingen.de
[4] Dipartimento di Scienze della Terra, Università degli Studi di Firenze, 50121 Firenze, Italy; alessandro.mondanaro@unifi.it
[5] Departament d'Història i Història de l'Art, Universitat Rovira i Virgili, 43002 Tarragona, Spain; adelbove@iphes.cat
[6] Institut Català de Paleoecologia Humana i Evolució Social (IPHES-CERCA), 43007 Tarragona, Spain
[7] Function, Evolution & Anatomy Research Lab, Zoology Division, School of Environmental and Rural Science, University of New England, Armidale, NSW 2351, Australia; gabriele.sansalone@uniroma3.it
[8] Dipartimento di Scienze Cardiovascolari, Respiratorie, Nefrologiche, Anestesiologiche e Geriatriche, Università degli Studi di Roma La Sapienza, 00185 Rome, Italy; paolo.piras@uniroma3.it
* Correspondence: marina.melchionna@unina.it
† Co-first authorship.

Abstract: The observation and the quantification of asymmetry in biological structures are deeply investigated in geometric morphometrics. Patterns of asymmetry were explored in both living and fossil species. In living organisms, levels of directional and fluctuating asymmetry are informative about developmental processes and health status of the individuals. Paleontologists are primarily interested in asymmetric features introduced by the taphonomic process, as they may significantly alter the original shape of the biological remains, hampering the interpretation of morphological features which may have profound evolutionary significance. Here, we provide a new R tool that produces the numerical quantification of fluctuating and directional asymmetry and charts asymmetry directly on the specimens under study, allowing the visual inspection of the asymmetry pattern. We tested this *show.asymmetry* algorithm, written in the R language, on fossil and living cranial remains of the genus *Homo*. *show.asymmetry* proved successful in discriminating levels of asymmetry among sexes in *Homo sapiens*, to tell apart fossil from living *Homo* skulls, to map effectively taphonomic distortion directly on the fossil skulls, and to provide evidence that digital restoration obliterates natural asymmetry to unnaturally low levels.

Keywords: asymmetry; *show.asymmetry*; fossil; virtual anthropology; geometric morphometrics; Arothron

1. Introduction

Most living organisms present bilateral symmetry, meaning that the left and right sides of the body represent an almost perfect reflection of one another about the medial plane. However, perfect symmetry is virtually absent in nature, and minor, localized deviations from perfect symmetry are common. Asymmetry can thus be defined as a deviation of the shape from a perfectly mirrored image of the counter-side of a bilateral object. The observation and quantification of asymmetry patterns in biological structures are keenly studied by evolutionary and developmental biologists, anthropologists, and paleontologists. There are three different types of asymmetries in living organisms: (i) fluctuating asymmetry,

(ii) directional asymmetry, and (iii) antisymmetry. The term fluctuating asymmetry (FA) applies to small left–right differences produced by developmental noises in the form of environmental and/or genetic stress [1]. Several studies identified FA as a good proxy for developmental instability. However, this assertion is still questioned, especially when it comes to the effect of habitat fragmentation, urbanization, and pollution on FA [2–6]. In humans, FA is usually linked to childhood diseases and poor genetic quality [7,8]. Different studies report a possible relationship between a mate's facial attractiveness and symmetry and usually support the notion that FA is higher in males than in females ([9–12], but see [13]). However, FA linkage to developmental disorders in our species remains contentious [14]. As an example, in a study carried out in the early medieval society from the Mikulčice settlement (Czech Republic), the higher degree of FA in females is deemed to be linked to the large variety of the female population due to patrilocality, although environmental effects cannot be ruled out [15].

Directional asymmetry (DA) refers to a skewed distribution of asymmetry when comparing the left to the right side of the body. DA has been largely observed in both vertebrates and invertebrates (i.e., the direction of coiling in gastropod shells, the presence of grossly unequal claws in male fiddler crabs [16]). Major examples of DA in humans pertain to handiness and brain lateralization, which in turn relates to the functioning of Broca's area for speech production [17]. Several investigations of DA in humans focused on differences occurring between males and females and usually support the notion that DA is higher in males [18,19]. DA was also used as an indicator of biomechanical loading in humans [15].

Antisymmetry (AS) is commonly defined as the inversion of the regular pattern of asymmetry, and it is widespread in both animals and plants [20]. The analysis of traits with antisymmetry may present a bimodal distribution in the most extreme manifestation, as in the case of left and right claw size in fiddler crabs. An extreme example of antisymmetry in humans is the condition known as *situs inversus*, which refers to the congenital mirrored position of most of the internal organs [21].

Studying and understanding asymmetry patterns also hold a prominent role in paleontology. Taphonomic and diagenetic processes (i.e., the postburial deformation of the organic material) can heavily affect the physical preservation of biological remains and obliterate their natural symmetry. The majority of fossils thence present damages and missing parts, as well as severe, plastic deformations due to compressive and shear forces. Incorrect identification of the nature of taphonomic distortions may misguide the recognition of diagnostic features, producing taxonomic and evolutionary misinterpretations [22,23]. More than DA and FA, which are virtually impossible to determine in the vast majority of fossil species, paleontologists are interested in quantifying the loss of biological symmetry and in identifying patterns of compression and distortion on the remains to guide the restoration of their original shape and the correct interpretation of diagnostic features. In the last few decades, with the rise of virtual paleontology, several methods of digital restoration were developed. Mirroring procedures [24–27], retrodeformation (i.e., the restoration of specimen's symmetry [28,29]), and target deformation [30] are all examples of digital manipulation procedures aiming to produce the genuine shape the remains had before taphonomy impinged on them. Assessing the reliability of these techniques is therefore crucial for paleontologists and anthropologists interested in virtual restoration.

A number of methodological strategies have been proposed to compute and discriminate between FA, DA, and AS by using geometric morphometrics data [19,31–34]. However, these strategies are generally limited in terms of visual outputs, mostly offering a 2D visualization, and/or require multiple steps to prepare the data before the asymmetry analyses can be conducted. The low visual rendering makes these approaches suboptimal in terms of interpreting the topology and regional variation in the intensity of the patterns of asymmetry and is of little help when the goal is to produce a sensible virtual restoration of the features paleontologists are most interested in.

Herein, we present a new function written in R language, named *show.asymmetry*, that allows users to visualize and measure the left–right differences of bilateral biological objects, while mapping the extent of asymmetry on the object surface and calculating levels of FA and DA where appropriate. To test *show.asymmetry*, we applied the tool to (i) visualize and assess levels of asymmetry in male and female *Homo sapiens* skulls from contemporary populations, (ii) identify patterns of asymmetry in human fossil specimens and compare them to modern humans, and (iii) test the effect of retrodeformation techniques in restoring the original biological symmetry.

2. Materials and Methods

2.1. show.asymmetry

The *show.asymmetry* algorithm is a landmark-based procedure embedded in the Arothron R package [35]. The function works with multiple landmark sets. As the first step, *show.asymmetry* splits each configuration in a left (L) and a right (R) half, following the specified indices for bilateral pairs of landmarks. The two halves are superimposed to each other via generalized Procrustes analysis (GPA) to exclude the non-shape-related differences and compute the rotation matrix to mirror, scale, and align the left side onto the right side or vice versa. By setting the argument *scale.sides*, the user may decide to apply the scaling process of the two halves during the Procrustes superimposition (see Table 1 for the detailed explanation of all arguments). As the default, scaling is not performed. The amount of shape difference that is not removed through the GPA process between the two halves is a measure of the shape differences between both sides. Asymmetry is computed as the square root of the sum of the squared distances between each landmark pair (L and R) as follows:

$$\text{asymmetry} = \sqrt{\sum_{i=1}^{n} \left(L_i - R_i \right)^2}$$

where L and R are the superimposed left and right landmark configurations and *n* is the number of landmarks per side. If the samples differ in terms of dimension (i.e., they belong to different species or genera, or they greatly vary in size), it may be useful to standardize the amount of asymmetry to unit size to compare them directly. Thus, in *show.asymmetry*, the total amount of asymmetry is divided by the maximum interlandmark distance of the sample configuration. This correction is triggered by the function's argument *scale.size*. In the case of specimens under analysis falling under discrete groups, *show.asymmetry* automatically retrieves the mean shapes for the groups indicated by the user.

The asymmetry pattern is automatically visualized on one half of the object surface by using *meshDist* function in 'Morpho' R package, [32], with the asymmetry values used as distance vector. The function also displays the two superimposed surfaces and, eventually, the local area differences between the two halves by using the algorithm embedded in the *localmeshdiff* function ('Arothron' R package, [35]). The area difference range for all the given specimens is rescaled into the 0–1 range to make them comparable. If no reference surface is provided, *show.asymmetry* uses the function *vcgBallPivoting* in 'Morpho' to reconstruct both L and R halves for visualization.

show.asymmetry further gives the possibility to perform a principal component analysis (PCA) on a new set of landmarks obtained by subtracting the mean from the left and mirrored right (or the other way around) side. The output from the PCA is used to decompose the total variance in two components describing the percentage of variation attributed respectively to DA (mean difference between sides) and FA (average differences around mean of asymmetry) (for details, see [31,36]).

The function retrieves the asymmetry vectors, the local area differences vector, the surfaces with levels of asymmetry mapped on a color scale, the PCA results, the asymmetric component of shape variance, and the percentage of DA and FA (see Table 2 for a detailed explanation).

Table 1. Explanation of the arguments of *show.asymmetry*.

Argument Name	Explanation
set	A single matrix k × m or a k × m × n array, where k is the number of points, m is the number of dimensions, and n is the sample size.
x	character: the species/specimens to be analyzed; names specified in the x argument must be included and coincide with the dimnames of the array.
pairs	A two-column data frame containing the indices (row numbers) of the bilateral landmarks.
scale.size	logical: if TRUE, the asymmetry will be corrected with the maximum interlandmark distance.
uniform.range	logical: if TRUE, the color range for the asymmetry visualization will be uniform among all specimens analyzed.
scale.sides	logical: if TRUE, the left and the right side will be scaled during the Procrustes superimposition process.
scale.ranges	logical: if TRUE, the vector of asymmetry values will be scaled from 0 to 1.
PCA	logical: if TRUE, a Principal Component Analysis is performed.
pcx	numeric: first PC axis to be visualized.
pcy	numeric: second PC axis to be visualized.
ref.sur	Reference surfaces to be used for the visualization; if ref.sur is NULL, the surfaces will be automatically reconstructed starting from the landmarks by using the *vcgBallPivoting* algorithm from Morpho R package (Schlager, 2017).
.from	numeric: minimum distance for the asymmetry to be colorized.
.to	numeric: maximum distance for the asymmetry to be colorized.
plot	logical: if TRUE, visualize result for asymmetry as 3D plot.
pal.dist	logical: if TRUE, the mesh area differences are displayed in a second 3D plot.
pal.areas	logical: if TRUE, the names of the species and/or the number of the node are displayed in the 3D plot.

Table 2. *show.asymmetry* value illustration.

Value	Explanation
asym	Vector of asymmetry values.
area.differences	Vector of area differences values.
asymmetry.surfaces	List of objects of mesh3d colorized according to the asymmetry values.
area.diff.surfaces	List of objects of mesh3d colorized according to the area differences values.
PCA	List object containing the mean shape, PC scores, PCs, and the variance table according to the output from Morpho::procSym.
asymmetric.component	The percentage of shape variance explained by asymmetry.
DA	The percentage of directional asymmetry.
FA	The percentage of the fluctuating asymmetry.

2.2. Case Studies

We applied and tested *show.asymmetry* on different case studies. First, we applied the function to a collection of sexed modern human crania. We compared levels of asymmetry in two different groups, male (N = 10) and female (N = 10), to observe if asymmetry patterns differ among sexes. We also computed a PCA on the asymmetric component as described in Section 2.1.

The second case study pertains to two fossil *Homo* skulls we studied to look at the patterns of taphonomic distortion. The two specimens refer to *Homo heidelbergensis* from Petralona and the *Homo neanderthalensis* from Saccopastore 1. The Neanderthal specimen shows extensive asymmetry in the parietotemporal region next to the slight clockwise rotation of the facial complex with respect to the neurocranium [29] (Figure 1).
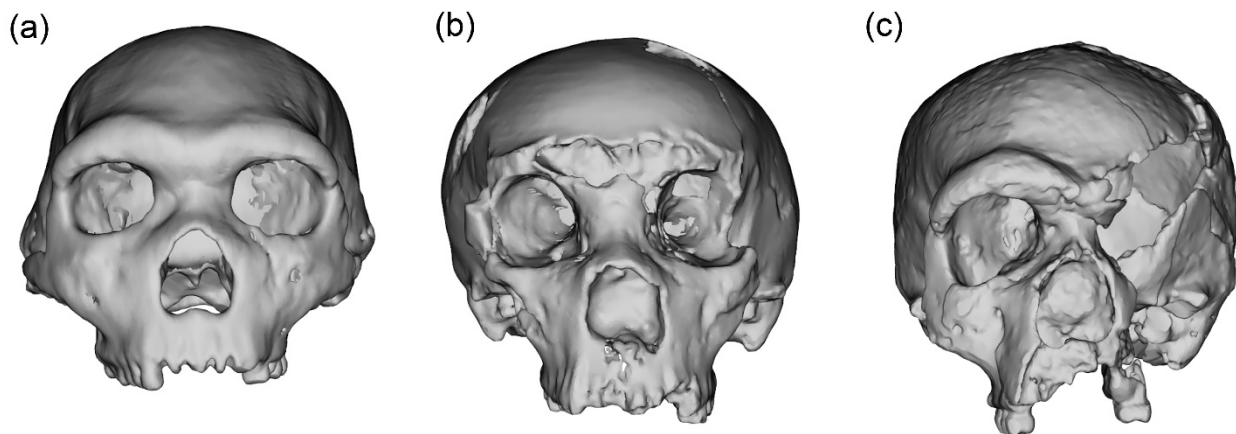
Figure 1. Fossil specimens for *show.asymmetry* case studies. (**a**) Petralona, (**b**) Saccopastore 1, and (**c**) Steinheim skulls.

Petralona represents a well-preserved *Homo heidelbergensis* skull discovered by Malkotsis and colleagues in 1959 in a cave site near the Petralona village (Thessaloniki, Greece). The cranium lacks the right zygomatic arch. The mastoid processes are broken. The upper portion of the sphenoid bone is missing. A wide opening intervenes in between the cranial and nasal cavities and the maxillary sinuses [37]. As highlighted by Rightmire [38], there are slight deformations of the vault. Although the frontal bone is undeformed, the right parietal bulges more than its left counterpart, and the right temporal squama is displaced laterally. The palate is rotated about the sagittal plane of the braincase, indicating some twisting of the facial skeleton towards its right side.

Saccopastore 1 was discovered in 1929 in the aggradational succession of the Aniene River Valley (Rome, Italy). The cranium is almost complete, although it lacks both zygomatic arches and the left orbital region is damaged. Some additional and severe damages were due to its accidental discovery in a gravel pit during construction works. The most extensive damage occurred to the browridge region, which is missing. The neurocranium also presents two pick stroke marks. For the application of *show.asymmetry*, the two holes were closed digitally, while the browridge could not be restored.

The last case study regards the application of *show.asymmetry* to evaluate the effect of retrodeformation on asymmetry. To avoid biases due to the inclusion of deformed specimens in morphometric analysis, or misinterpretation of morphological traits, paleontologists have applied the so-called retodeformation protocol to artificially restore symmetry in digital models [23,26,29,39]. This symmetrization procedure is powerful and effective, yet it cannot discriminate between taphonomic distortion and natural asymmetry. We decided to test *show.asymmetry* on a highly deformed specimen before and after the retrodeformation procedure to see if the retrodeformed specimen shows a lower than expected level of asymmetry (as judged by comparison to living *Homo sapiens* specimens) and whether *show.asymmetry* captures this essential feature of the retrodeformation process. We used the Steinheim skull case-study presented in [40] (this volume). Steinheim cranium was found in 1933 in a gravel pit 70 km north of Steinheim an der Murr (Baden-Württemberg, Germany) and, despite a longstanding debate, is commonly attributed to *Homo heidelbergensis*, or otherwise linked to the Neanderthal lineage [41,42].

2.3. Data Preparation

We acquired 50 anatomical landmarks on each modern human skull specimen on the entire cranial surface (e.g., facial complex, neurocranium, and cranial base). We placed 500 equidistant surface semilandmarks on the left side only of a reference sample. We slid the semilandmark on the entire sample of 20 specimens following the protocol included in 'Morpho' [32]. Then, we mirrored the slid configurations to the other side and projected them on the surfaces after a GPA step rotating semilandmark configuration accordingly to the set of bilateral landmarks.

Concerning fossil specimens, we manually sampled bilateral landmarks on Petralona and Saccopastore by using Amira software (version 5.4.5 [43]) (see Supplementary Materials for the full detailed description of landmarks). We created decimated patches by cutting half of the skull, and then we removed the damaged parts on each surface (i.e., the browridge region from Saccopastore 1). For each patch, we retrieved the coordinates of the vertices and used them as semilandmarks. As we needed bilateral points, we symmetrized the semilandmarks on the opposite side and slid them along the surface by using manually placed landmarks as a reference. The manipulation of landmarks and semilandmarks was performed by using the R Cran software (version 4.0.5).

For the Steinheim case study, we used both the original and the retrodeformed patches from the study presented in [40] (this volume).

3. Results

The comparison between the two modern samples highlighted that male individuals show 40% more asymmetry on average. Such enhanced asymmetry is especially evident in the temporoparietal area, the occipital region, and the maxillary bone (Figure 2a). Student's t-test on asymmetry vectors for male and female mean shapes indicates these differences are significant ($t = -9.7703$, p values < 0.001). The asymmetric component is 2.7% of total shape variance. This component is primarily made up of FA, which accounts for 93.6% of it, meaning FA represents 2.53% (93.6 times 2.7) of the total shape variance.
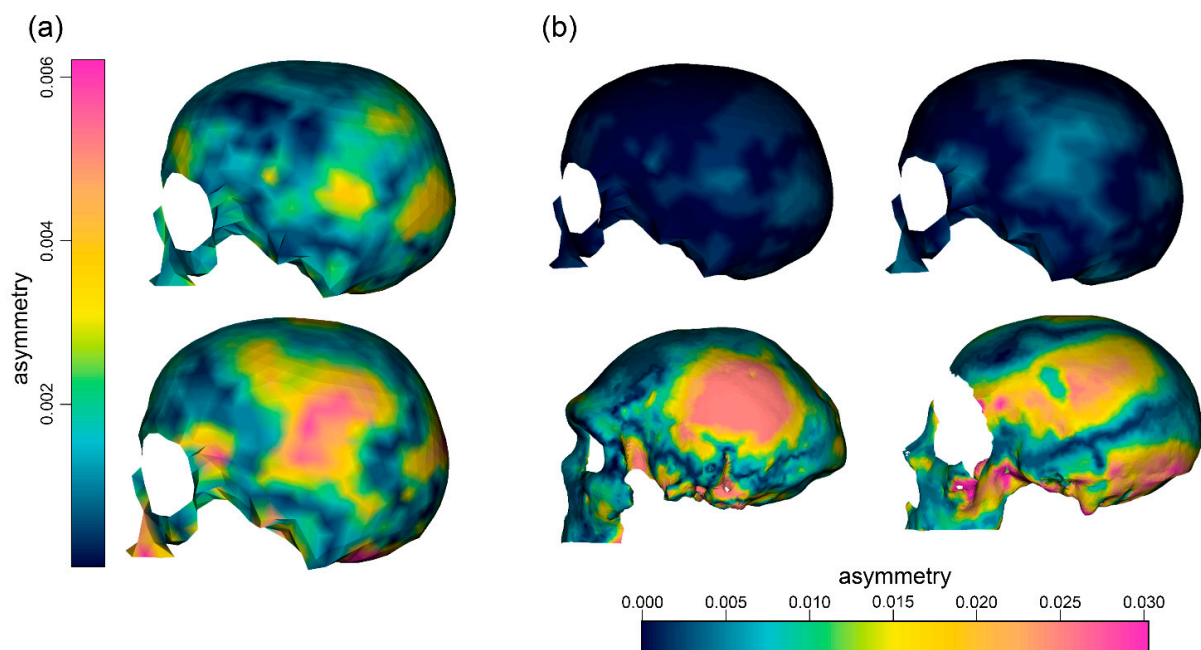

Figure 2. Visualization of the degree of asymmetry obtained with *show.asymmetry*. (**a**) Comparison between the mean shape of female and male modern humans (upper row and bottom row, respectively). The range of asymmetry goes from the minimum to the maximum value of asymmetry between the two samples. (**b**) Comparison between the mean shape of female and male modern humans (upper row left and right, respectively) and Petralona and Saccopastore 1 (lower row, left and right respectively). The range of asymmetry is scaled between samples.

When modern humans are compared to Petralona and Saccopastore 1, their degree of asymmetry appears diminutive (Figure 2b). Petralona shows a marked pattern of asymmetry in the temporoparietal area, while the facial complex appears to be more symmetric than the cranial vault. Saccopastore 1 presents a directional pattern of asymmetry with a peak corresponding to the zygomatic and lateral maxillary areas, due to the bad status of preservation of the left side of the splanchnocranium. Both patterns agree well with what has been reported in the literature regarding these specimens [29,37].

Overall, Steinheim is the most asymmetric specimen (Figures 3 and 4). As expected by the descriptions provided in [44], the skull shows extensive deformations on the splanchnocranium, whereas shape was less affected in its rearmost part. However, in keeping with our hypotheses, after the retrodeformation process, the level of asymmetry is close to zero. Lastly, the modern human crania show a minor level of asymmetry when contrasted with the asymmetry level measured in fossil specimens. (Figures 3 and 4).
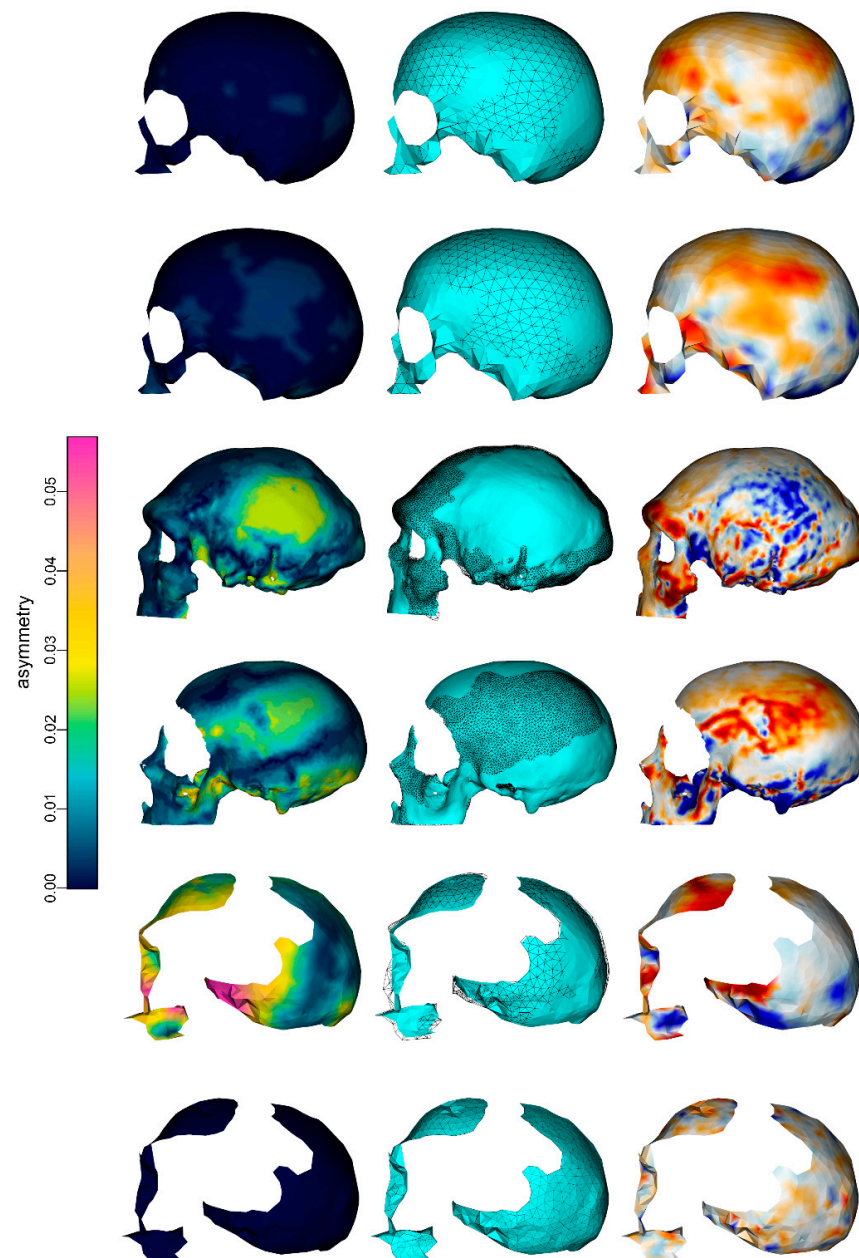

Figure 3. Graphical results produced by *show.asymmetry*. The first column shows the asymmetry pattern in terms of vertex distances between the two superimposed halves (the shared scale is shown on the left). The second column shows the superimposition of the two halves (in this case, the left side is the cyan surfaces, while black wireframe corresponds to the superimposed right side). The third column represents the local area differences between the left and the right side; the scale goes from blue to red (meaning expansion and contraction, respectively), and it is not shared. From top to bottom: mean shape of female individuals, mean shape of male individuals, Petralona, Saccopastore 1, Steinheim before retrodeformation, Steinheim after retrodeformation.
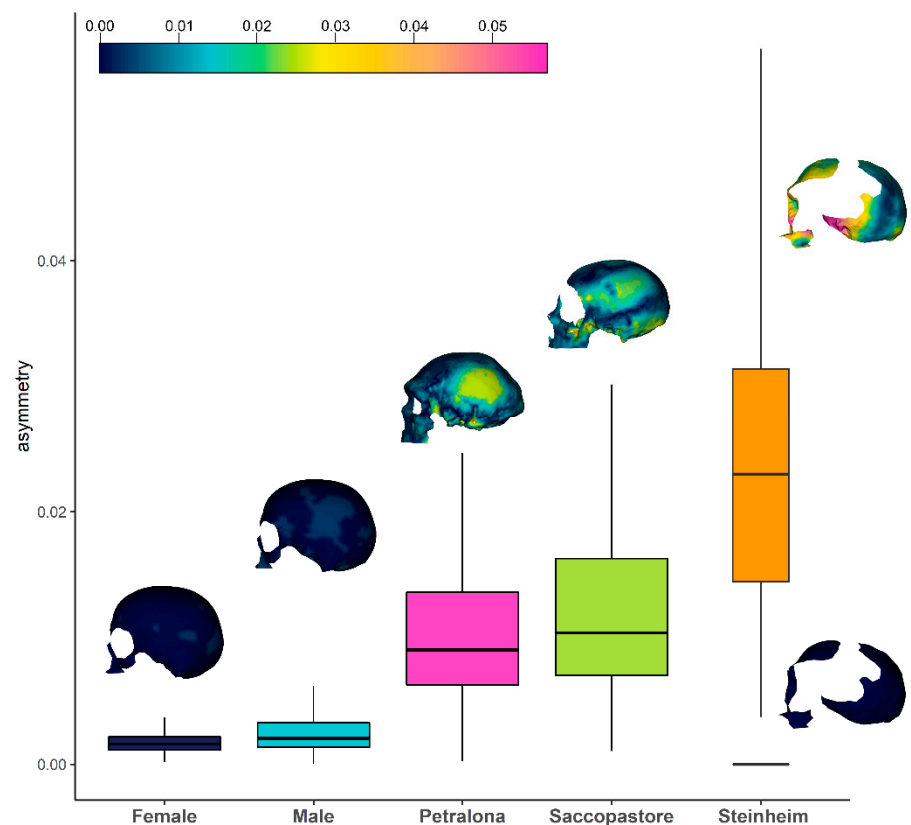
Figure 4. Boxplot of the comparison of asymmetry values for the analyzed samples. From left to right: *Homo sapiens* female mean shape, *Homo sapiens* male mean shape, Petralona, Saccopastore 1, and Steinheim (before and after the retrodeformation procedure). The color gradient for the asymmetry displayed in the crania is shown.

The time requested to run all the four case studies was 3.95 s and in particular: Petralona 0.93 s, Saccopastore 0.81 s, Homo sapiens 1.40 s, Steinheim 0.81 s. Speed tests were run with a laptop Intel Core-i7 10875H (2.30 GHz and 32 GB RAM).

4. Discussion

There are several strategies available to evaluate asymmetry from landmark-based datasets [31,34]. Despite the presence of different methods, none of these offer a fully integrated tool to calculate and especially to map asymmetry from and to mesh-based models. Furthermore, the new function *show.asymmetry* is able to evaluate asymmetry in both multiple datasets (array) and single specimens (matrix), returning colored meshes showing the pattern of asymmetry in two different ways: the 3D map of Euclidean distances and the 3D map of local variations of area.

For example, in the R package 'geomorph' [45], the function *bilat.asymmetry* provides a 3D scatterplot of the distortion of landmarks or the 3D colorless meshes warped according to the detected pattern of asymmetry. Furthermore, landmark clouds can be useful or easy to read when dealing with a small number of points or with relatively simple 3D structures. However, when using complex 3D geometries (such as crania) and/or large numbers of landmarks, other graphical outputs, such as heatmaps, are a more welcome option [34]. Nonetheless, even built-in functions such as *bilat.symmetry* require multiple steps to be performed by the users in order to be implemented. Specifically, the two sets of coordinates defining the two sides are mirror images, and hence they must be reflected for landmark alignment (multiplication of the raw data matrix by −1 is required). On the same page, the approach described by Neubauer et al. [34] requires performing the singular value decomposition (SVD) of the raw data matrix of asymmetric vectors rather than

performing a standard PCA of the mean-centered data. These steps must be performed before testing for the presence of any asymmetry pattern, increasing the chances of misuse and lengthening the time to perform the entire set of analyses.

When dealing with fossil specimens, it must be considered that taphonomic processes may sensibly alter the original shape of fossil remains. Whereas cracks and missing parts are undisputable accidents of the preservation process, the compressive and shear stresses acting upon the remains over prolonged periods of time may bring about plastic deformations that could be misinterpreted as 'natural'. This, in turn, may have important consequences on the correct recognition of the phylogenetic position and taxonomy of the remains [22,23]. For instance, the 'roofed' appearance of the neurocranium in the Steinheim skull was interpreted as evidence of its plesiomorphic condition [46] but may be better indicative of taphonomic alteration [40] (Buzi et al., this volume). A similar misinterpretation might have complicated the interpretation of Ceprano *Homo heidelbergensis* calvarium [47]. Digital restorations help in driving the restoration of the original shapes yet obliterate true object symmetry (sensu [31]) and are uninformative as to where and to what extent asymmetry applies in the first place. The algorithm of *show.symmetry* provides exactly this piece of information and therefore helps to understand the processes behind the taphonomic distortions and their total amount. As demonstrated in the first case study, male *Homo sapiens* skulls are on average more asymmetric than female skulls. Whereas this result does not generalize and was not thought to provide an answer to a complicated question as to whether females, as compared to males, really tend to have a lower level of cranial asymmetry [15], it stills shows that *show.asymmety* retrieves even small differences between closely knit individuals. Similarly, *show.asymmetry* confirms that retrodeformation procedures actually reduce cranial symmetry below the natural level, even applied to a highly deformed skull such as Steinheim. Importantly, the tool successfully estimates and maps levels and direction of asymmetric deformations directly on the fossil remains, which may provide critical information when the recognition of the processes behind the deformation and the proper fossil restoration are at the stake.

5. Conclusions

show.asymmetry estimates and charts patterns of asymmetry on three-dimensional digital models. It straightaway performs a correction for size variation within the sample, decomposes asymmetry into its directional and fluctuating components, and maps asymmetry on the three-dimensional surface, allowing users to grasp immediate visual information on the intensity, topology, and direction of departures from perfect symmetry. Through the three different case studies presented here, we showed the functioning of *show.asymmetry* algorithm with different datasets, from recent human individuals to human fossil specimens.

References

1. Klingenberg, C.P. A developmental perspective on developmental instability: Theory, models and mechanisms. In *Developmental Instability: Causes and Consequences*, 1st ed.; Polak, M., Ed.; Oxford University Press: Oxford, UK, 2003; Volume 1, pp. 14–34.
2. Marchand, H.; Paillat, G.; Montuire, S.; Butet, A. Fluctuating asymmetry in bank vole populations (Rodentia, Arvicolinae) reflects stress caused by landscape fragmentation in the Mont-Saint-Michel Bay. *Biol. J. Linn. Soc.* **2003**, *80*, 37–44. [CrossRef]
3. Oleksyk, T.K.; Novak, J.M.; Purdue, J.R.; Gashchak, S.P.; Smith, M.H. High levels of fluctuating asymmetry in populations of Apodemus flavicollis from the most contaminated areas in Chornobyl. *J. Environ. Radioact.* **2004**, *73*, 1–20. [CrossRef]
4. Lazić, M.M.; Carretero, M.A.; Crnobrnja-Isailović, J.; Kaliontzopoulou, A. Effects of environmental disturbance on phenotypic variation: An integrated assessment of canalization, developmental stability, modularity, and allometry in lizard head shape. *Am. Nat.* **2015**, *185*, 44–58. [CrossRef]
5. Lezcano, A.H.; Rojas Quiroga, M.L.; Liberoff, A.L.; Van der Molen, S. Marine pollution effects on the southern surf crab Ovalipes trimaculatus (Crustacea: Brachyura: Polybiidae) in Patagonia Argentina. *Mar. Pollut. Bull.* **2015**, *91*, 524–529. [CrossRef]
6. Chirichella, R.; Rocca, M.; Brugnoli, A.; Mustoni, A.; Apollonio, M. Fluctuating asymmetry in Alpine chamois horns: An indicator of environmental stress. *Evol. Ecol.* **2020**, *34*, 573–587. [CrossRef]
7. Van Dongen, S.; Gangestad, S.W. Human fluctuating asymmetry in relation to health and quality: A meta-analysis. *Evol. Hum. Behav.* **2011**, *32*, 380–398. [CrossRef]
8. Weisensee, K.E. Assessing the relationship between fluctuating asymmetry and cause of death in skeletal remains: A test of the developmental origins of health and disease hypothesis. *Am. J. Hum. Biol.* **2013**, *25*, 411–417. [CrossRef] [PubMed]
9. Schaefer, K.; Fink, B.; Grammer, K.; Mitteroecker, P.; Gunz, P.; Bookstein, F.L. Female appearance: Facial and bodily attractiveness as shape. *Psychol. Sci.* **2006**, *48*, 187–204.
10. Pflüger, L.S.; Oberzaucher, E.; Katina, S.; Holzleitner, I.J.; Grammer, K. Cues to fertility: Perceived attractiveness and facial shape predict reproductive success. *Evol. Hum. Behav.* **2012**, *33*, 708–714. [CrossRef]
11. Muñoz-Reyes, J.A.; Pita, M.; Arjona, M.; Sanchez-Pages, S.; Turiegano, E. Who is the fairest of them all? The independent effect of attractive features and self-perceived attractiveness on cooperation among women. *Evol. Hum. Behav.* **2014**, *35*, 118–125. [CrossRef]
12. Foo, Y.Z.; Simmons, L.W.; Rhodes, G. Predictors of facial attractiveness and health in humans. *Sci. Rep.* **2017**, *7*, 39731. [CrossRef] [PubMed]
13. Komori, M.; Kawamura, S.; Ishihara, S. Averageness or symmetry: Which is more important for facial attractiveness? *Acta Psychol.* **2009**, *131*, 136–142. [CrossRef]
14. Graham, J.H.; Özener, B. Fluctuating asymmetry of human populations: A review. *Symmetry* **2016**, *8*, 154. [CrossRef]
15. Bigoni, L.; Krajíček, V.; Sládek, V.; Velemínský, P.; Velemínská, J. Skull shape asymmetry and the socioeconomic structure of an early medieval central european society. *Am. J. Phys. Anthropol.* **2013**, *150*, 349–364. [CrossRef]
16. Palmer, A.R. Symmetry breaking and the evolution of development. *Science* **2004**, *306*, 828–833. [CrossRef] [PubMed]
17. Cantalupo, C.; Hopkins, W.D. Asymmetric Broca's area in great apes. *Nature* **2001**, *414*, 505. [CrossRef]
18. Claes, P.; Walters, M.; Shriver, M.D.; Puts, D.; Gibson, G.; Clement, J.; Baynam, G.; Verbeke, G.; Vandermeulen, D.; Suetens, P. Sexual dimorphism in multiple aspects of 3D facial symmetry and asymmetry defined by spatially dense geometric morphometrics. *J. Anat.* **2012**, *221*, 97–114. [CrossRef] [PubMed]
19. Ekrami, O.; Claes, P.; White, J.D.; Weinberg, S.M.; Marazita, M.L.; Walsh, S.; Shriver, M.D.; Van Dongen, S. A multivariate approach to determine the dimensionality of human facial asymmetry. *Symmetry* **2020**, *12*, 348. [CrossRef]
20. Palmer, A.R. Antisymmetry. In *Variation*; Elsevier: Amsterdam, The Netherlands, 2005; p. 359-XXIV.
21. Vingerhoets, G.; Gerrits, R.; Verhelst, H. Atypical brain asymmetry in human situs inversus: Gut feeling or real evidence? *Symmetry* **2021**, *13*, 695. [CrossRef]
22. Sansom, R.S.; Wills, M.A. Fossilization causes organisms to appear erroneously primitive by distorting evolutionary trees. *Sci. Rep.* **2013**, *3*, 2545. [CrossRef]
23. Lautenschlager, S. Reconstructing the past: Methods and techniques for the digital restoration of fossils. *R. Soc. Open Sci.* **2016**, *3*, 160342. [CrossRef]
24. Gunz, P.; Mitteroecker, P.; Neubauer, S.; Weber, G.W.; Bookstein, F.L. Principles for the virtual reconstruction of hominin crania. *J. Hum. Evol.* **2009**, *57*, 48–62. [CrossRef]
25. Benazzi, S.; Bookstein, F.L.; Strait, D.S.; Weber, G.W. A new OH5 reconstruction with an assessment of its uncertainty. *J. Hum. Evol.* **2011**, *61*, 75–88. [CrossRef]
26. Benazzi, S.; Gruppioni, G.; Strait, D.S.; Hublin, J.J. Technical Note: Virtual reconstruction of KNM-ER 1813 *Homo habilis* cranium. *Am. J. Phys. Anthropol.* **2014**, *153*, 154–160. [CrossRef]
27. Zollikofer, C.P.E.; Ponce de León, M.S.; Lieberman, D.E.; Guy, F.; Pilbeam, D.; Likius, A.; Mackaye, H.T.; Vignaud, P.; Brunet, M. Virtual cranial reconstruction of Sahelanthropus tchadensis. *Nature* **2005**, *434*, 755–759. [CrossRef] [PubMed]

28. Tallman, M.; Amenta, N.; Delson, E.; Frost, S.R.; Ghosh, D.; Klukkert, Z.S.; Morrow, A.; Sawyer, G.J. Evaluation of a new method of fossil retrodeformation by algorithmic symmetrization: Crania of papionins (primates, cercopithecidae) as a test case. *PLoS ONE* **2014**, *9*, e100833. [CrossRef] [PubMed]

29. Schlager, S.; Profico, A.; Di Vincenzo, F.; Manzi, G. Retrodeformation of fossil specimens based on 3D bilateral semi-landmarks: Implementation in the R package "Morpho". *PLoS ONE* **2018**, *13*, e0194073. [CrossRef]

30. Cirilli, O.; Melchionna, M.; Serio, C.; Bernor, R.L.; Bukhsianidze, M.; Lordkipanidze, D.; Rook, L.; Profico, A.; Raia, P. Target Deformation of the Equus stenonis Holotype Skull: A Virtual Reconstruction. *Front. Earth Sci.* **2020**, *8*, 247. [CrossRef]

31. Mardia, K.V.; Bookstein, F.L.; Moreton, I.J. Statistical assessment of bilateral symmetry of shapes. *Biometrika* **2000**, *87*, 285–300. [CrossRef]

32. Schlager, S. Morpho and Rvcg—Shape Analysis in R: R-Packages for Geometric Morphometrics, Shape Analysis and Surface Manipulations. In *Statistical Shape and Deformation Analysis: Methods, Implementation and Applications*; Zheng, G., Li, S., Székely, G., Eds.; Academic Press: Cambridge, MA, USA, 2017; pp. 217–256, ISBN 9780128104941.

33. Klingenberg, C.P. Analyzing fluctuating asymmetry with geometric morphometrics: Concepts, methods, and applications. *Symmetry* **2015**, *7*, 843–934. [CrossRef]

34. Neubauer, S.; Gunz, P.; Scott, N.A.; Hublin, J.J.; Mitteroecker, P. Evolution of brain lateralization: A shared hominid pattern of endocranial asymmetry is much more variable in humans than in great apes. *Sci. Adv.* **2020**, *6*, eaax9935. [CrossRef]

35. Profico, A.; Buzi, C.; Castiglione, S.; Melchionna, M.; Piras, P.; Veneziano, A.; Raia, P. Arothron: An R package for geometric morphometric methods and virtual anthropology applications. *Am. J. Phys. Anthropol.* **2021**, *176*, 144–151. [CrossRef]

36. Profico, A.; Zeppilli, C.; Micarelli, I.; Mondanaro, A.; Raia, P.; Marchi, D.; Manzi, G.; O'Higgins, P. Morphometric maps of bilateral asymmetry in the human humerus: An implementation in the R package morphomap. *Symmetry*. under review.

37. Seidler, H.; Falk, D.; Stringer, C.; Wilfing, H.; Müller, G.B.; Zur Nedden, D.; Weber, G.W.; Reicheis, W.; Arsuaga, J.L. A comparative study of stereolithographically modelled skulls of Petralona and Broken Hill: Implications for future studies of middle Pleistocene hominid evolution. *J. Hum. Evol.* **1997**, *33*, 691–703. [CrossRef] [PubMed]

38. Rightmire, G.P. Middle Pleistocene *Homo* Crania from Broken Hill and Petralona: Morphology, metric comparisons, and evolutionary relationships. In *Human Paleontology and Prehistory*; Springer: Berlin/Heidelberg, Germany, 2017; pp. 145–159.

39. Cuff, A.R.; Rayfield, E.J. Retrodeformation andmuscular reconstruction of ornithomimosaurian dinosaur crania. *PeerJ* **2015**, *3*, e1093. [CrossRef]

40. Buzi, C.; Profico, A.; Di Vincenzo, F.; Harvati, K.; Melchionna, M.; Raia, P.; Manzi, G. Retrodeformation of the Steinheim cranium: Insights into the evolution of Neanderthals. *Symmetry* **2021**, *34*, 1611. [CrossRef]

41. Hublin, J.J. The origin of Neandertals. *Proc. Natl. Acad. Sci. USA* **2009**, *106*, 16022–16027. [CrossRef] [PubMed]

42. Mounier, A.; Caparros, M. The phylogenetic status of *Homo heidelbergensis*—A cladistic study of Middle Pleistocene hominins. *Bull. Mem. Soc. Anthropol. Paris* **2015**, *27*, 110–134. [CrossRef]

43. Stalling, D.; Westerhoff, M.; Hege, H.C. Amira: A highly interactive system for visual data analysis. *Vis. Handb.* **2005**, *1*, 749–767. [CrossRef]

44. Prossinger, H.; Seidler, H.; Wicke, L.; Weaver, D.; Recheis, W.; Stringer, C.; Müller, G.B. Electronic removal of encrustations inside the steinheim cranium reveals paranasal sinus features and deformations, and provides a revised endocranial volume estimate. *Anat. Rec. Part B New Anat.* **2003**, *273*, 132–142. [CrossRef] [PubMed]

45. Adams, D.; Collyer, M.; Kaliontzopoulou, A.; Baken, E. Geomorph: Software for Geometric Morphometric Analyses. R Package Version 4.0. Available online: https://cran.r-project.org/package=geomorph (accessed on 21 July 2021).

46. Schwartz, J.H.; Tattersall, I. *The Human Fossil Record*; John Wiley & Sons: New York, NY, USA, 2005; Volume 2, ISBN 0471319287.

47. Bruner, E.; Manzi, G. CT-based description and phyletic evaluation of the archaic human calvarium from Ceprano, Italy. *Anat. Rec. Part A Discov. Mol. Cell. Evol. Biol.* **2005**, *285*, 643–657. [CrossRef]